Multiple technical observations of the atmospheric boundary layer structure of a red warning haze episode in Beijing

Yu Shi[1,2], Fei Hu[1,2], Guangqiang Fan[3], and Zhe Zhang[1,2]

[1]State Key Laboratory of Atmospheric Boundary Layer Physics and Atmospheric Chemistry,Institute of Atmospheric Physics, Chinese Academy of Sciences,Beijing 100029
[2]University of Chinese Academy of Sciences, Beijing 100049
[3]Key Laboratory of Environmental Optics and Technology, Anhui Institute of Optics and Fine Mechanics,Chinese Academy of Sciences, Hefei 230031

Correspondence: Fei Hu (hufei@mail.iap.ac.cn)

Abstract. The study and control of air pollution need to detect the structure of atmospheric boundary layer (ABL) in order to understand the mechanism of interaction between atmospheric boundary layer and air pollution. However, when extreme pollution occurs,the detection of atmospheric boundary layer structure is very scarce. Beijing, the capital of China, has experienced a severe haze pollution in December 2016. The city issued its first red air pollution warning of this year (the highest $PM_{2.5}$

5 concentration was later monitored to exceed $450 \mu g\ m^{-3}$). In this paper, the vertical profiles of wind, temperature, humidity and extinction coefficient (reflecting aerosol concentration), as well as ABL heights and turbulence quantities under heavy haze pollution are analyzed, with collected data from Lidar, wind profile radar (WPR), radiosonde, 325-meter meteorological tower (equipped with 7-layer ultrasonic anemometer and 15-layer low frequency wind, temperature and humidity sensors) and some other ground observations. ABL heights obtained by three different methods based on Lidar extinction coefficient data (H_c)

10 are compared with the heights calculated from radiosonde temperature data (H_θ) and from WPR wind speed data (H_u). The results show that increase of water vapor has greatly promoted the hygroscopic growth of aerosols, the corresponding extinction coefficients also increased significantly. The PBL heights H_θ and H_u of heavy haze pollution days were generally lower than those of clean days, but H_c increased. Turbulent activities were great inhibited during haze pollution, time changes of both friction velocity (u_*) and turbulent kinetic energy (TKE) have obvious inverse correlation with that of $PM_{2.5}$. The results of

15 this paper could provide some reference for the parameterization of the boundary layer height and turbulent diffusion process in the numerical model of severe air pollution.

1 Introduction

Air pollution has an important impact on human health,weather,climate and ecological environment (Seinfeld and Pandis, 1997; Brook et al., 2004; Ding et al., 2013; Wang et al., 2014a; Zhang et al., 2015a). The pollutants emitted by human activities are

20 mainly confined to the atmospheric boundary layer (ABL) which is the lowest part of the troposphere and about 1∼2 km from the ground. In particular, fog and haze, which have a great influence on visibility and air quality, mainly occur in the ABL (Cao et al., 2004; Chan and Yao, 2008; Fu et al., 2008; Liu et al., 2012). Because the formation, evolution, and diffusion of air

pollutants are closely related to ABL structure and turbulence characteristics (Zhang et al., 2011; Wei et al., 2018), research on ABL is important for understanding air pollution mechanisms and developing pollution control strategies. On the other hand, relationship between ABL and atmospheric pollution is very complicated and involves multiscale nonlinear physical and chemical processes, both theoretical research and numerical simulation have encountered difficulties (Sun et al., 2013;

5   Huang et al., 2014; Wang et al., 2014b; Miao et al., 2018). Therefore, it is very necessary to obtain first-hand information from observation experiments.

Regarding air pollution, there have been many observational experiments in the world, especially air pollution in the ABL over urban areas (i.e., urban boundary layer). For example, COST715 (European Cooperation in the Field of Scientific and Technical Research)(Fisher et al., 2001), URBAN 2000 (Allwine et al., 2002),Joint Urban 2003 (Wang et al., 2007),MIRAGE

10   2006 (Lance et al., 2012)and SURF (Liang et al., 2018).

Meteorological tower is one of the best platforms to detect the ABL structure under the condition of atmospheric pollution (Quan and Hu, 2009; Sun et al., 2015; Ren et al., 2018). Although its height is limited, the boundary layer is basically in a stable boundary layer when heavy pollution occurs, and the ABL height is low, so it is easy to detect by tower. Conventional meteorological instruments and turbulence instruments installed at different heights above the tower can obtain the information

15   of stable boundary layer structure and turbulence diffusion parameters (Katul et al., 1995). The traditional detection methods include tethered balloon, radiosonde, wind profiler radar (WPR) and so on, which can detect higher heights (Grimsdell and Angevine, 1998; Andreas et al., 2000; Kalapureddy et al., 2007; Li et al., 2015; Han et al., 2018). In the past Decades, aerosol laser radar (Lidar) has been used more and more widely. It can be used to retrieve the vertical distribution of particles from the backscattering data of Lidar (Wang et al., 2012; Summa et al., 2013; Jiannong et al., 2013; Bravo-Aranda et al., 2017).

20   It is impossible to obtain information on the boundary layer structure and the interrelationship of pollutants in atmospheric pollution (especially in heavy haze) unilaterally by means of the above-mentioned technical means, and it is necessary to carry out comprehensive observations simultaneously.

From 14 to 22 December 2016, Beijing, the capital of China, experienced a serious haze pollution process. The government issued the highest air pollution warning (red alert) during this period. Beijing is a densely populated city with an area of

25   about 396 square kilometers (see Fig.1). Despite vigorous pollution control measures taken by the government, the average $PM_{2.5}$ concentration per hour has rose from $20\mu g\ m^{-3}$ to more than $450\mu g\ m^{-3}$ (seen in Table.1) in just five days. What is the mechanism of such severe air pollution? This requires a comprehensive and in-depth analysis of the weather background, pollutant emissions, regional transport and physicochemical transformation mechanisms, as well as the interaction between haze and boundary layer structures (Huang et al., 2014; Sun et al., 2014; Ding et al., 2016). There have been some previous

30   studies on the haze events in Beijing area (Li et al., 2017; Sheng et al., 2018; Wang et al., 2018), especially the physical and chemical mechanism analysis based on the observation data of high-space and multi-element of the tower (Sun et al., 2006; Guo et al., 2016).

The purpose of this paper is to investigate the ABL structure and turbulence characteristics during the a red haze warning period in year 2016 by means of tower, Lidar, WPR and radiosonde. The contents include a brief introduction to the weather

35   background and basic facts of the heavy haze pollution, observation sites and techniques, analysis of boundary layer wind,

temperature, humidity profiles, extinction coefficients (reflecting the concentration of haze particles), and determination of ABL heights obtained by different detection techniques. The vertical distributions of turbulent quantities are also studied. Finally, further research considerations are also given.

2 Observation sites, instruments and data

5   The ABL observation data of this paper are mainly obtained in three locations in Beijing. One is located at the Institute of Atmospheric Physics (IAP) of the Chinese Academy of Sciences, where there are a 325 meters heigh meteorological towers and a Lidar. The second is about 600 meters away from the east side of the tower, and there is a WPR. The third is the observatory of the Beijing Meteorological Bureau, which is about 20 kilometers away from the tower. There are conventional ground meteorological observations and radiosonde, which belong to the WMO station(ZBAA in Fig.1). The above observation

10   sites are shown in Figure 1. The time used in this paper is the local station time and the observational instruments and data are introduced as follows:

Figure 1. The location of the observation site,red circle:IAP(325m tower, Lidar, WPR), grey circle:WMO radiosonde observation satttion(ZBAA). An pollution observation station is about 2km in the north-east of the tower. Beijing is a densely populated city with an area of about 396 square kilometers

1) Meteorological tower of IAP is 49 meters above sea level and 325 meters high, which is located in the (39°58'N, 116°22'E, 49m above sea level) between the Beijing North Third Ring Road and North Fourth Ring Road from August 1979. A total of 15 observation platforms (at 8, 15, 32, 47, 65, 80, 103, 140, 160, 180, 200, 240, 280 and 320m) are set up on the tower, and wind

15   speed(MetOne,USA), wind direction(MetOne,USA), temperature (HC2-S3,Switzerland) and humidity (HC2-S3, Switzerland) observation instruments are mounted on each platform. Moreover, 7 sets of three-dimensional ultrasonic anemometers (Wind

Master,Gill,USA) and water vapor / carbon dioxide analyzers (LI-7500,USA) are also installed on the tower (at 8, 15, 47, 80, 140, 200 and 280m). All turbulence data sampling frequency is 10 Hz. All of the tower data are averaged for 20 minutes. A detailed description of the meteorological tower can be found in (Al-Jiboori and Fei, 2005) and (Chen et al., 2018) , and on the website (http://view.iap.ac.cn:8080/imageview/).

5   2) The extinction coefficients were measured by Lidar (AGHJ-I-Lidar,China) installed underneath 325m tower. The Lidar could provide backscattering signals at wavelength of 532nm and 355nm with a vertical resolution of 7.5m and a temporal resolution of about 5∼10min.Due to technical failure, the lidar data were missing from 11:00 on December 19 to 09:00 on December 20, 2016;

3) Wind speed and wind direction were also monitored by means of a WPR (Airda3000,China) during red-alert pollution
10   period. In this paper, the temporal resolution of WPR is 5min, and the vertical resolution is 50m below 1000m and 90m above the 1000m;

4) The twice daily (08:00 and 20:00 in Beijing time) radiosonde vertical profile data were got from the University of Wyoming website(http://weather.uwyo.edu/)for Beijing station which named ZBAA in international code.And surface visibility, pressure and other meteorological elements were obtained from University of Wyoming website(http://weather.uwyo.edu/
15   surface/meteorogram/index.shtml) with a temporal resolution of half an hour(position is shown in Fig.1, ZBAA);

5) Surface measurements of six kinds of air pollutants with a temporal resolution of one hour can be found on the official website of the Beijing Environmental Protection Agency (http://beijingair.sinaapp.com/). The data used in this paper comes from the environmental monitoring station (Olympic Sports Center Station) which is nearest station to the tower(about 2km in the northeast).

20 ## 3   Results and discusses

3.1   Surface observation of haze and meteorological conditions

From 14 to 22 December 2016, a complete haze pollution was observed in Beijing area(seen in Table 1). The generation, accumulation and elimination of $PM_{2.5}$ were recorded. We can see that, from 20 to 21 December, the hourly average $PM_{2.5}$ concentration almost maintained around $400\mu g\ m^{-3}$ within 48 hours, which greatly exceeded the highest level of pollution
25   (i.e. $250\mu g\ m^{-3}$) in the air pollution standards of China's State Environmental Protection Administration . Figure.2 shows the concentration time series of $PM_{2.5}$, wind speed and direction, temperature, relative humidity(RH), surface pressure and visibility of this heavy haze pollution process.

Generally, the visibility plays an representative index of air quality and atmospheric diffusion capacity (Zhang et al., 2015b). Figure.2 shows that when the concentration of $PM_{2.5}$ became high, visibility was deteriorating rapidly. Visibility of clean days was mainly greater than 10km, and if $PM_{2.5}$ concentration was about 200∼300$\mu g\ m^{-3}$, visibility then reduced to 2∼5km, or
30   even when $PM_{2.5}$ reached about $400\mu g\ m^{-3}$, visibility dropped sharply to 1km or hundreds of meters. The surface pressure suggests that the air pressure decreased approximately from 1035hPa to 1023hPa, and in general, Beijing was controlled by a weak high-pressure system during pollution episode. The RH of ground observation had a significant diurnal variation and

Table 1. Daily average data of six major air pollutants in Beijing during heavy pollution from 14 to 23 December 2016: $PM_{2.5}$,PM_{10},NO_2,SO_2 and O_3 (their units are all $\mu g\ m^{-3}$);CO(mg m^{-3}).Data sources: http://beijingair.sinaapp.com/

Date	Air Quality	AQI index	$PM_{2.5}$	PM_{10}	NO_2	SO_2	CO	O_3
2016-12-14	Good	60	24	38	42	9	0.74	32
2016-12-15	Good	83	25	51	40	9	0.85	31
2016-12-16	Slightly Polluted	274	101	134	87	20	2.07	8
2016-12-17	Heavy Polluted	351	184	211	102	30	3.14	5
2016-12-18	Serious Polluted	337	219	245	100	24	3.42	7
2016-12-19	Serious Polluted	306	214	247	107	22	3.88	7
2016-12-20	Serious Polluted	342	365	422	133	8	7.67	4
2016-12-21	Serious Polluted	363	393	429	152	10	7.97	4
2016-12-22	Moderately Polluted	325	93	170	45	6	1.95	39
2016-12-23	Good	55	31	42	43	7	0.74	26

there existed obvious anti-correlation between RH and temperature. From 20 to 21 December, the diurnal variation of the temperature and relative humidity in heavy pollution was greatly suppressed, indicating that heavy pollution can indeed affect the temperature of the ground through the process of pollutants or radiation process (Gao et al., 2015), and the RH of the ground was also enhanced to 90~100% during this period. The increase of RH, on the one hand, is due to the decrease of temperature, on the other hand, is the result of the surge of the water vapour. For example, in the early morning ,temperature difference between 17 and 20 December was very small, the RH of 17 December was about 80%, while the RH in the early morning of 20 December was almost 100%, indicating the increase of water vapour content in Beijing area at this time. The surface wind speed during polluted episode was almost less than 2m s^{-1}, basically regarded as a stagnant weather system. And in the winter, the occurrences of northern wind along with high wind speed could often improve the air quality over Beijing area significantly(Sheng et al., 2018).
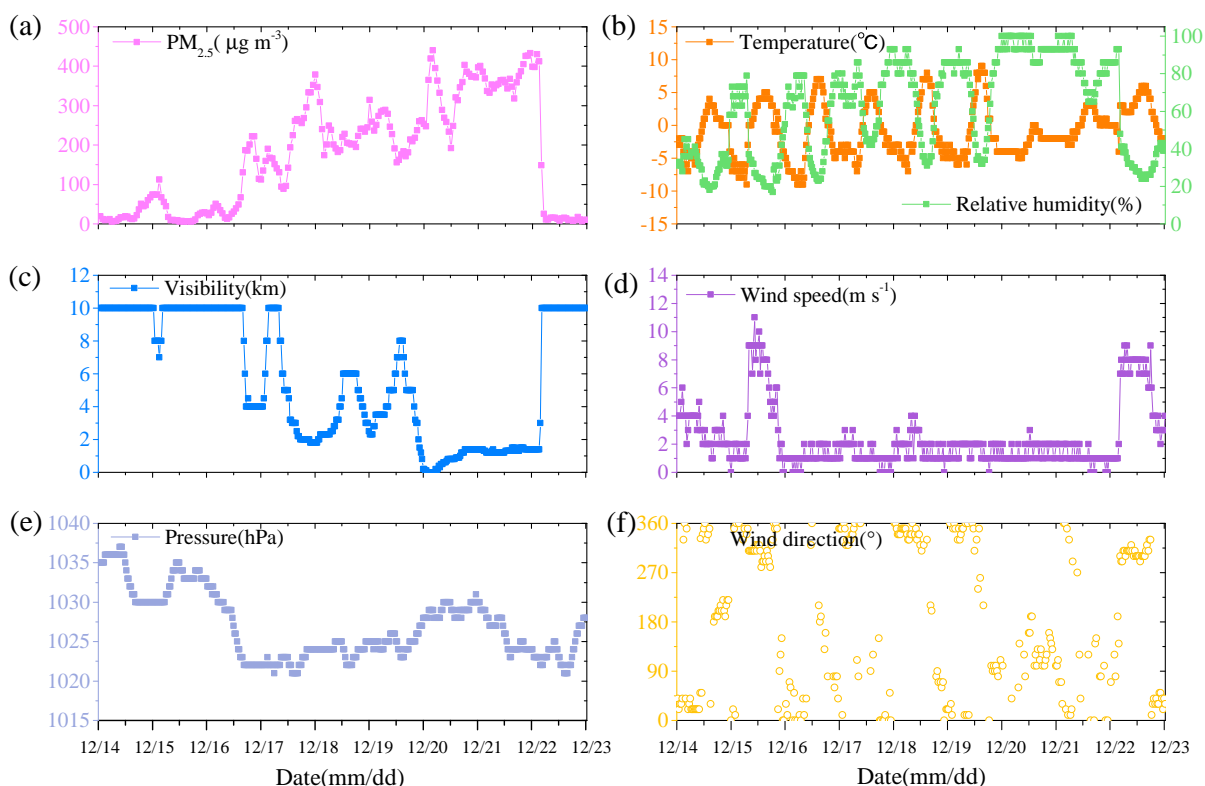
Figure 2. Time series of ground level $PM_{2.5}$(a),relative humidity and temperature(b),visibility(c),wind speed(d),surface pressure(e) and wind direction(f)during 14 to 22 December 2016,the units of those meteorological parameters are $\mu g\ m^{-3}$,%,°C,km,m s^{-1},hPa and ° respectively.

3.2 Boundary layer heights observed by Lidar, WPR and radiosonde

Generally, the atmospheric boundary layer can be divided into the daytime convective mixing layer and the night stable boundary layer. In the morning the well-mixed convective boundary layer (CBL) is growing and often reaches its maximum height in the early afternoon. In the afternoon the CBL gradually changes into a neutral boundary layer. Figure.3 shows the evolution
5 of the ABL heights measured by Lidar, WPR and radiosonde respectively. The most essential definition of the ABL height is the height at which the influence of the earth's surface on the lower troposphere disappears. This influence applies not only to conventional meteorological elements but also to the turbulence quantities, or even more the substances in the atmosphere such as aerosols, water vapor or nonreactive tracer gases (Seibert et al., 2000). Various pollutants and water vapor in the ABL are much higher than that in the free atmosphere and it can be approved from the vertical distribution of extinction coefficient.
10 Therefore, there often exists obvious aerosol concentration gradient between the boundary layer and the free atmosphere. The background in figure.3 is the extinction coefficient detected by the double wave long three channel aerosol Lidar located in IAP, and the extinction coefficient can act as an index of the vertical distribution of aerosol concentration in the atmosphere

(Boers and Eloranta, 1986). We used the three popular methods, which are gradient method (Lidar_gra) (Flamant et al., 1997), standard deviation method (Lidar_std) (Hooper and Eloranta, 1986) and wavelet method (Lidar_wav) (Cohn and Angevine, 2000; Davis et al., 2000; Brooks, 2003) respectively to extract the boundary layer heights from the extinction coefficients. The ABL height determined by Lidar is represented by H_c.

5   The Lidar_gra method is defined by the height of atmosphere where the gradient of the Lidar extinction coefficient reaches its steepest nagative value in this article. The standard deviation of extinction coefficient reflects the degree of the dispersion of the Lidar echo signals at different heights. The top of the planetary boundary layer is the intersection of the air in the boundary layer and the free atmosphere, which leads to a strong signal change on the top of the boundary layer. This paper defines the height of the maximum standard deviation of signals as the ABL height. The Lidar_wav method can also be used to detect the

10   abrupt change of signals, so we have used the Haar wavelet and taken the height in which wavelet coefficient is maximum as the height of the ABL height.
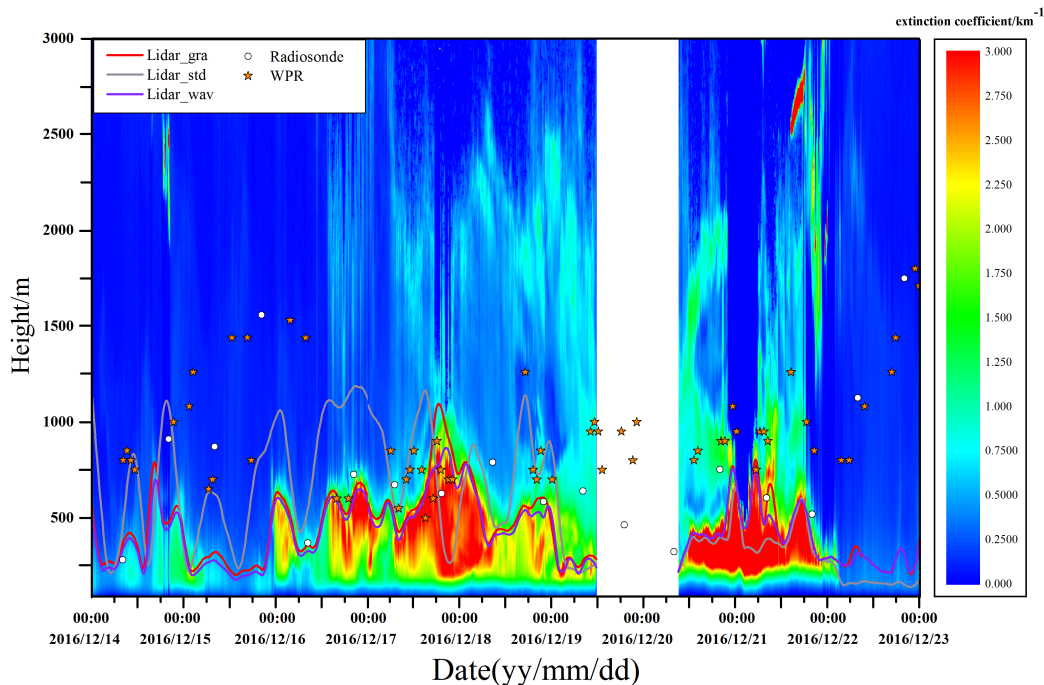
Figure 3. Temporal and spatial variation of extinction coefficient (shaded,unit:km^{-1}) from 14 to 23 December,2016 and ABL height(m) determined by different instruments. Red line (Lidar_gra), grey line(Lidar_std),purple line(Lidar_wav) represent ABL height determined by Lidar using gradient method,standard deviation method, and wavelet method respectively. White points:ABL height determined by radiosonde;Five-pointed star:ABL height determined by WPR.It should be noted that the blank part of the extinction coefficient is due to a technical failure, and the lidar data were missing from 11:00 on December 19 to 09:00 on December 20.

The determination of the ABL height by means of Lidar is based on the vertical profiles of extinction coefficient, namely the aerosol concentration. When the concentration of $PM_{2.5}$ is high, the weakening effect of aerosol particles on laser is stronger. The ABL height determined by Lidar_gra and Lidar_wav were almost the same, with a correlation coefficient of nearly 95%. During 16 to 18 December and 20 to 21 December, the ABL height were about 500∼750m. Furthermore, the ABL height

5 determined by Lidar_std method was slightly higher than that of both methods. During the heavy pollution episode days (20 to 21 December), the extinction coefficient quickly exceeded $3km^{-1}$ above 250m from the ground. Perhaps due to the accumulation of pollutants, H_c did not seem to reduce in these days. When the atmosphere was relatively clean, such as 15 or 22 December, the aerosol concentration was low and the extinction coefficient of Lidar had no obvious transformation zone. The ABL heights obtained by these methods based on the Lidar were obviously lower than those of other instruments. If we

10 continue to use Lidar to determine the height of the boundary layer, it will be obviously distorted. Therefore, the continuous observation of the ABL height can be attained by means of other instruments or improved method based on Lidar.

3.3 Boundary layer structure observed by radiosonde

Radiosonde is the most widely used conventional meteorological observation method in the world. The white points in figure.3 are the ABL height determined by the radiosonde data. The potential temperature(θ) of the radiosonde is calculated by the

15 formula: θ=T+$\gamma_d z$, where γ_d=0.00975K m^{-1}, T is the measured temperature. As pointed out in many previous studies, "the most widely used approach for the determination of the PBL height and structure both in daytime and nighttime is represented by the identification of local maxima in the potential temperature vertical gradient profiles as measured by radiosondes" (Summa et al., 2013; Sorbjan, 1989). In this article, the maximum potential temperature gradient is defined as the ABL height (Hennemuth and Lammert, 2006), and is expressed by H_θ (seen blue dotted lines in the Fig.4). We have selected some profiles

20 of θ and RH measured by radiosonde to get characteristics of H_θ. The atmosphere stratification of potential temperature and RH could affect the distribution characteristics of aerosol concentration, and further affect extinction coefficient. So, vertical profiles of the extinction coefficient observed by the Lidar at the corresponding moments were also displayed.

As shown in figure.4, the pollution episode was often accompanied by inversion layer, namely the vertical gradient of PT is positive, implying that the atmosphere was basically stable. Air pollutants are generally blocked below the inversion layer and

25 are not easily diffused to high levels. Figure.4 shows that H_θ at 20:00 on 16 December was about 727m, where the potential temperature was about 280K and the RH was about 20%, and the extinction coefficient has also been reduced to 0.7km^{-1}. Due to the cooling effect of the surface longwave radiation, the ground inversion layer was formed from the surface and this inversion layer depth was about 100m. Owing to the remaining characteristics of mixed layer during the daytime, the potential temperature of 100∼600m changed a little with the height. Until about 700m from the ground, another temperature

30 inversion layer appeared. The maximum negative value of the extinction coefficient gradient appeared at about 500m at this time, and the extinction coefficient below 727m was much higher than that above 727m, indicating that aerosol particles were mainly concentrated below the inversion layer (Baumbach and Vogt, 2003), and H_θ calculated by the radiosonde was basically consistent with H_c determined by Lidar.
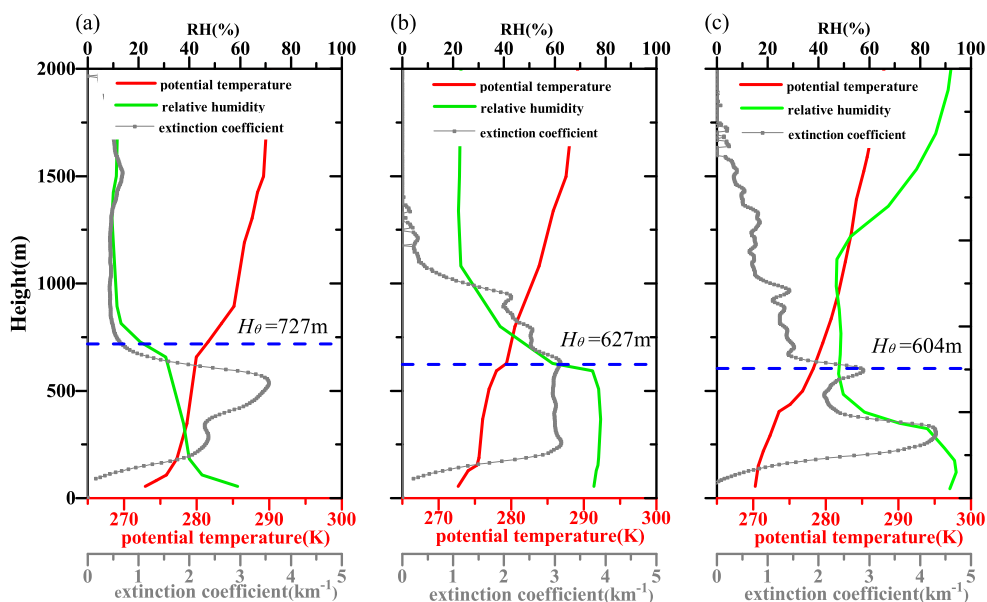
Figure 4. Vertical profiles measured at ZBAA meteorological station.(a) 20:00,16 December, 2016 (b)20:00, 17 December, 2016(c) 08:00 21 December,2016.Red line: potential temperature(K);Green line:RH(%);Grey line:extinction coefficient(km^{-1});blue dotted line:ABL height determined by radiosonde expressed in H_θ(m).

    At 20:00 on 17 December, the ground inversion layer has also begun to form. The H_θ was about 627m, and the potential temperature of this level was still around 280K, however the RH reached nearly 60%. Below this height, the whole atmosphere layer has formed a high humidity layer with RH nearly 80% from the ground, in addition, the corresponding extinction coefficient has also increased significantly. The extinction coefficient between 250∼600m was almost 3km^{-1}, revealing that the

5 concentration of aerosols increased significantly. Combined with the wind direction at this time(Fig.5d), it is clearly illustrated that the transport of the easterly wind has brought abundant water vapour, which promoted the hygroscopic growth of aerosol particles. At 08:00 on 21 December, the potential temperature distribution in the morning was different from 20:00, and the surface temperature has begun to increase as the receiving of solar radiation. The ground inversion layer has disappeared and the H_θ was about 604m. The RH below 500m was nearly 95%, and meanwhile the maximum value of the extinction coeffi-

10 cient, which exhibited bimodal, reached nearly 4km^{-1}. The altitude where extinction coefficient reached the peak at high layer was near to H_θ approximately. By means of analyzing and comparing H_c and H_θ, it can be found that when the concentration of PM$_{2.5}$ was high, the accumulation of pollutants was mainly accompanied by the inversion layer in the atmosphere. At the inversion layer, it was easier to appear the larger value of the potential temperature gradient. Even though the H_c represents the aerosol scattering information, and H_θ stands for potential temperature characteristics, there existes a good correlation

15 between them, with a correlation coefficient about 72%. However, when the atmosphere was clean, the aerosol concentration was obviously reduced and the inversion layer was not so significant. As shown in Figure.3, H_θ was significantly higher than the H_c determined by three methods based on Lidar extinction coefficient.

3.4 Boundary layer structure observed by WPR

The ground is the most important sink of atmospheric momentum and the wind speed is zero at the surface. The wind speed changes gradually from the surface to the geostrophic wind at high altitude, and the wind information extracted from the WPR has been widely used to determine the ABL height (Cohn and Angevine, 2000). There exist many different methods to estamte

5   the ABL height form wind profiles. In this paper, we use the height of the low level maximum wind speed as the ABL height, and expressed the height in H_u (Banta, 2008; Pichugina and Banta, 2010; Devara et al., 1995).

As shown in Figure.3, H_u was much higher than H_c, especially during the cleaning day, when the H_u was about 1500m. With the increase of PM$_{2.5}$ concentration, H_u also decreased, that is, the height of the low level maximum wind velocity would also decrease when the atmosphere is polluted. In that case, H_u, H_c and H_θ were very close.

10   In order to further understand the H_u determined by the WPR and clarify the wind structure of the whole ABL, the wind profile information from the ground to the high layer were given in this paper. As exhibited in Figure.5, the wind speeds below 1000m were not more than 6m s^{-1} on 17 December, and the H_u determined by the WPR was between 750~1000m. At 12:00 it was a typical "nose" profile distribution according to the wind profile, that is, there is a maximum value in the middle of the wind profile. The wind direction profiles show that the wind direction from the ground to about 750m belonged to the north-east

15   wind ($0° \sim 90°$), and the wind direction above 750m belonged to the north-west wind ($270° \sim 360°$). Furthermore, the wind directions from 750~2000m basically maintained stable in the north-west directions, which can be considered to be close to the geostrophic winds. At this time, the height of the maximum wind speed fitted well with height of the wind direction began to change into geostrophic wind. In addition to 12:00 on 17 December, at other four moments, there were almost entirely the north-eastern winds below 1000m, and the wind directions began to transform into the north-west winds at different heights.

20   The wind speed has increased to some extent on 21 December, and there were also typical "nose" type wind speed distributions at 00:00, 08:00 and 20:00. From the ground to 2500m, there was steady south-west wind at 00:00, and the maximum wind speed appeared about 900m. At this time, the extinction coefficient was also very low above 750m(shown in Fig.4), demonstrating that pollutants were also gathered below the height of H_u. At 12:00, the wind speed began to decrease slightly from the ground, and there was no obvious change after about 1100m where the wind speed was about 4m s^{-1}. Except for

25   00:00 on 21 December when south-west wind prevailed from the ground to the high altitude, wind directions have changed to the north-west at other moments, although the wind speeds were not very high below 500m, and wind speed maximum values occurred at the height around 1000m.

The wind directions of the 22 December were north-west from the low to higher layer, but the distribution of wind velocity profiles was different from that of 21 December. The wind speeds had no significant maximum value area, and the maximum

30   wind speed of 500m approached close to 12m s^{-1}. According to the extinction coefficient distribution (seen in Fig.3), the PM$_{2.5}$ concentration was greatly reduced on that day. H_u determined by the WPR and H_θ obtained by radiosonde were relatively close at this time, and both were far higher than H_c.
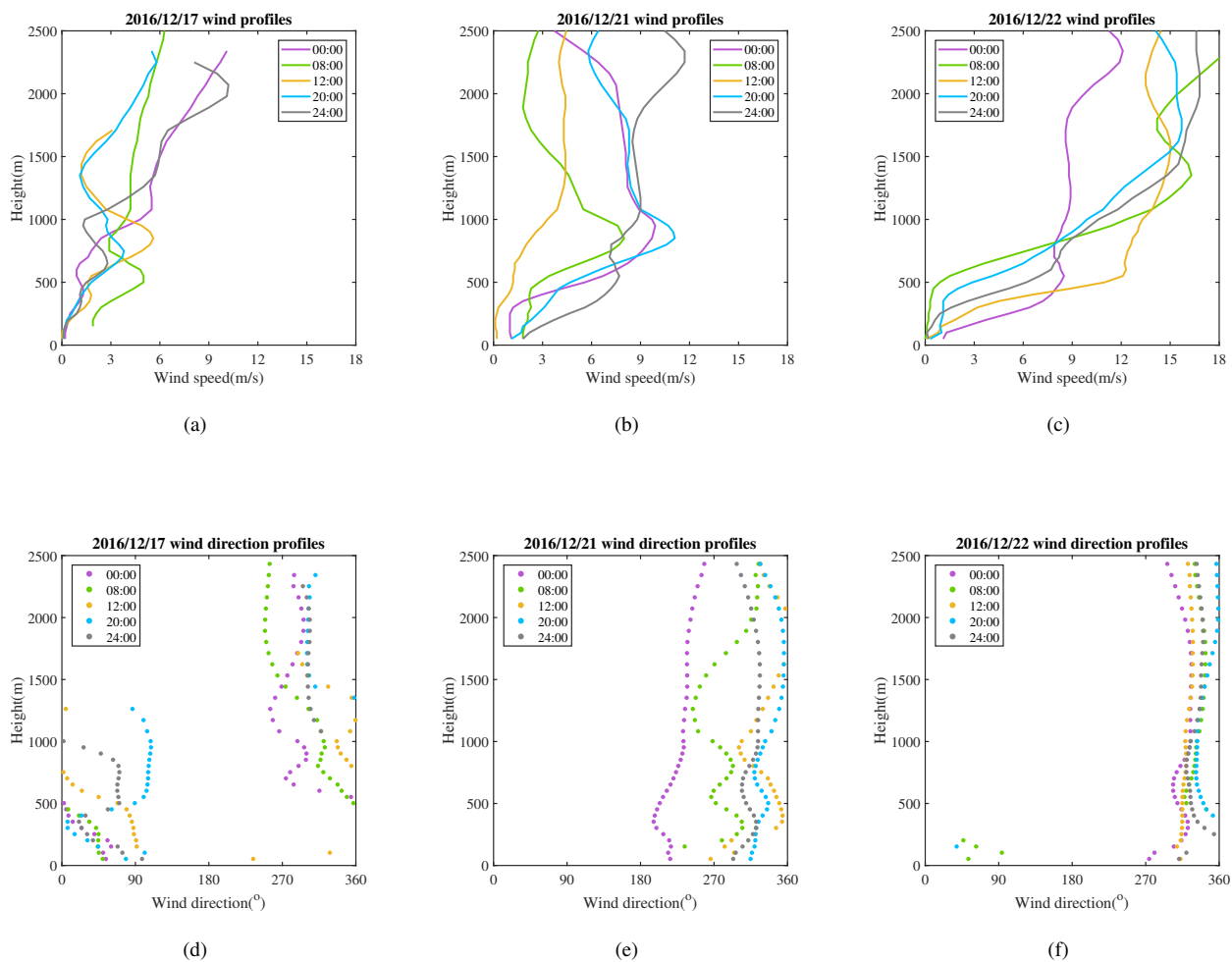
Figure 5. Vertical profiles of wind speed(m s^{-1}) and wind direction($°$) observed by WPR.(a)and(d):16 December,2016;(b)and(e):21 December,2016; (c)and(f):22 December,2016.

3.5 Boundary structure and turbulence quantities observed by 325m tower

As shown in Figure.6, both turbulent kinetic energy (TKE) and friction velocity (u$_*$) on 140m and 280 m were inversely correlated with ground level PM$_{2.5}$ concentration. The TKE and u$_*$ can be calculated as follows (Stull, 1988): $TKE = \frac{1}{2}(\overline{u'^2}+\overline{v'^2}+\overline{w'^2})$; $u_* = (\overline{u'w'} + \overline{v'w'})^{1/4}$. The maximum TKE during clean days (15 to 16 December) can reach about 7m^2 s^{-2} at 140m, while the TKE of haze days (17 to 21 December) decreased sharply to very small values. After entering the heavy haze pollution period, TKE maintained at a relatively small level, and the change of TKE was not so significant when the concentration of PM$_{2.5}$ increased from 200$\sim$400μg m^{-3}. On the other hand, the time series of u$_*$ was slightly different from that of TKE. It seems that the inverse correlation between u$_*$ and PM$_{2.5}$ was more obvious than that of TKE during the

heavy pollution period. In fact, even during heavy haze, a slight fluctuation (diurnal variation) of $PM_{2.5}$ concentration can be observed, and the diurnal variation of u_* was opposite to that of $PM_{2.5}$ phase.

(a)   (b)
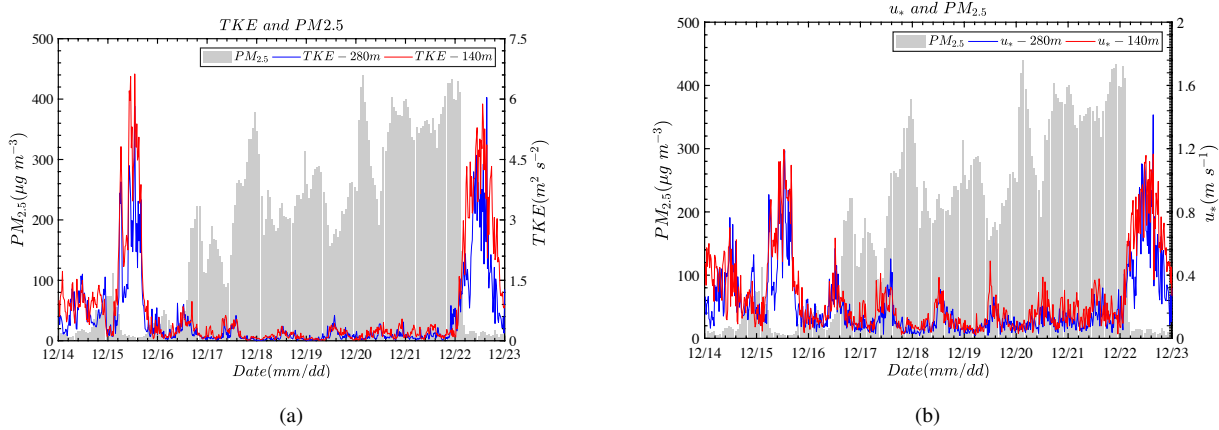
Figure 6. Time series of(a)turbulent kinetic energy(m^2 s^{-2}) and (b)friction velocity(u_*,m s^{-1}) at 140m(red line)and 280m(blue line),$PM_{2.5}$($\mu g\ m^{-3}$) concentration are also drawn in the figures(grey column).

In order to understand the vertical structure characteristics of the ABL observed by the tower during the pollution and clean episodes, the profiles of wind, potential temperature(θ), TKE, sensible heat flux($\overline{w'\theta'_v}$) and third order of vertical velocity

5 ($\overline{w'^3}$) in the lower boundary layer are also given. At night, the wind speed profile in the clear day was basically logarithmic distribution and the potential temperature changed little from the ground to about 300m. As for turbulent quantities, TKE also gradually decreased from about 70m, and the sensible heat flux was basically negative and the $\overline{w'^3}$ was the largest at 140m. On the polluted day, the wind speed from the lower to the upper layer was less than 2m s^{-1}. At this time, the change of potential temperature was not very large from the ground to about 200m, indicating that the atmosphere basically maintained the neutral

10 stratification. There was an obvious inversion layer cap until about 200m from the surface. TKE and $\overline{w'^3}$ were basically maintained near zero. Note that, at this time the sensible heat flux above 80m almost remained at zero. Near the ground, the sensible heat flux was a little positive, demonstrating that when the pollution occurred, especially when the inversion layer existed, the heat flux transport was suppressed. At night, the surface longwave radiative cooling effect was restrained to a certain extent, and the weakening of turbulence activities would aggravate the pollution situation again.
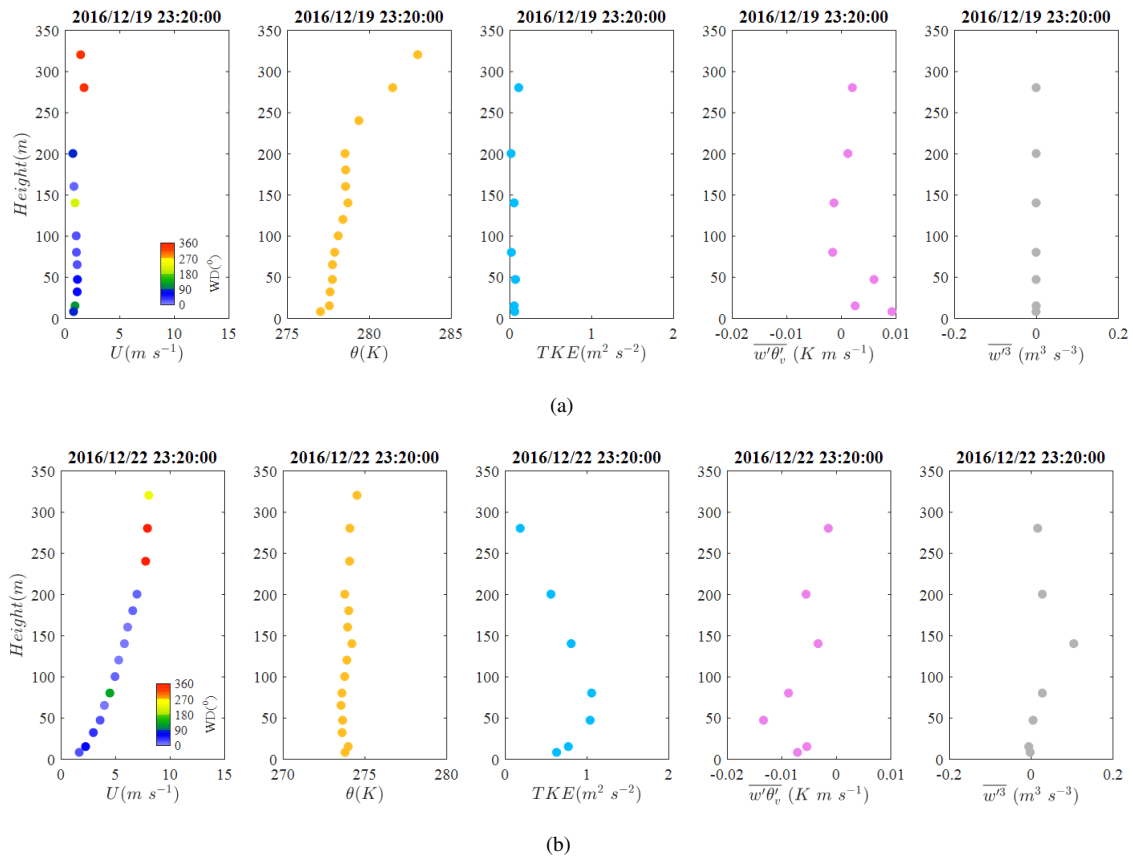
Figure 7. Vertical profiles of wind speed(U),wind direction(WD),potential temperature(θ),turbulent kinetic energy(TKE), sensible heat flux($\overline{w'\theta_v'}$) and third order moment of vertical velocity($\overline{w'^3}$) at 23:20 on 19 December,2016(a)and 22 December,2016(b).

According to the concentration of $PM_{2.5}$, the haze pollution situation can be divided into different grades. The statistical mean values of surface visibility(Vis), wind speed (U), RH, ABL height and the turbulent fluctuations are also calculated. As shown in the Table2, the statistical averages further confirm the conclusions of the previous analysis, such as when the concentration of $PM_{2.5}$ is high, visibility and wind speed decrease but RH increases significantly. Our results show that because of the accumulation of aerosol particles, H_c is even heightened slightly but H_c reduces by about 300m.The turbulence quantities also exhibit a decreasing trend during haze pollution episode,further demonstrating that turbulent activities are inhibited to a certain extent.

Table 2. The averaged value of visibility(Vis),wind speed(U),relative humidity(RH), ABL height(H_u,H_c), turbulent kinetic energy(TKE), friction velocity(u_*), momentum flux($\overline{u'w'}$),and sensible heat flux($\overline{w'\theta'_v}$) of different pollution degree. According to the "Technical Specification for Air Quality Index(HJ 633-2012)"issued by China National Environmental Protection Agency ,based on $PM_{2.5}$ concentration,the air pollution level can be divided into five levels, i.e. good($0\sim75\mu$g m^{-3}),slilghtly polluted($75\sim115\mu$g m^{-3}),moderately polluted($115\sim150\mu$g m^{-3}),heavily polluted($150\sim250\mu$g m^{-3}),seriously polluted($>250\mu$g m^{-3})

Quality Level	Vis (km)	U (m s^{-1})	RH (%)	TKE (m^2 s^{-2})	u_* (m s^{-1})	$\overline{u'w'}$ (m^2 s^{-2})	$\overline{w'\theta'_v}$ (K m s^{-1})	H_u (m)	H_c (m)
Good	9.9	4.0	39	1.23	0.31	0.08	0.0115	1124	358
Slightly	5.8	1.5	73	0.22	0.15	0.02	0.0022	837	484
Moderately	6.7	1.3	64	0.51	0.2	0.03	0.0032	750	502
Heavily	4.6	1.67	63	0.16	0.12	0.00045	0.0078	873	510
Seriously	2.0	1.38	81	0.15	0.11	0.0057	0.0038	844	518

4 Conclusions

In this paper, a red warning haze pollution process from 14 to 22 December 2016 in Beijing was studied by using various observational techniques. The atmospheric boundary layer structure and turbulence characteristics are the focus of this paper. Observational techniques include not only remote sensing techniques, e.g. Lidar and WPR, but also direct measurement tech-

5 niques, e.g. ground-based radiosonde and the 325m meteorological tower. Our research results show that, during the heavy haze pollution period, the Beijing area was controlled by the stagnant weather system. At 08:00 on 17 December, the confluence of north-easterly winds brought external pollutants and abundant water vapour to Beijing. Therefore, the relative humidity within 600m increased significantly, and further greatly promoted the hygroscopic growth of $PM_{2.5}$. The height of ABL height observed by Lidar(H_c) was about 500∼750m. Our present study shows that H_c did not seem to reduce during heavy pollution

10 episode due to the accumulation of pollutants. Based on the potential temperature gradient method, the ABL height calculated by radiosonde(H_θ) was in good agreement with H_c, with a correlation coefficient close to 72%. The ABL height (H_u) determined by WPR was basically higher than that of H_c, and H_u decreased obviously when heavy pollution occurred, closer to H_c and H_θ. The low level TKE, u_* and $PM_{2.5}$ were observed to be inversely related according to the tower. The turbulent fluxes varied very little with altitude, but the sensible heat flux was even slightly positive near the surface, indicating that the cooling

15 effect is inhibited by the long-wave radiation from the ground. Consequently,the suppression of turbulence will lead to further serious pollution.

Although different boundary layer heights can be obtained by various techniques, it seems that the ABL height measured by Lidar can better reflect the pollution accumulation during heavy haze pollution, and the ABL height measured by radiosonde is also in good agreement with the H_c measured by Lidar, which is useful for the study of atmospheric pollution boundary

20 layer based on conventional observations. Highly significant, our research found that the ABL height measured by WPR(H_u) is high. However, since the definition of ABL height observed by different means is essentially different in this class, they have their respective roles and significance.

Our future work will try to establish the parameterization of the relationship between friction speed and $PM_{2.5}$ concentrition, as they exhibit strong statistical correlations (negative correlations), for use in numerical models of air pollution. In addition, it

25 is also meaningful to explore the correlation between the dynamic, thermal and material (concentration) boundary layer heights (expressed by H_u, H_θ and H_c respectively) through more observations.

Competing interests. All the authors have declared that no competing interests exist

Acknowledgements. The authors thank Dr.Aiguo Li from the Institute of Atmospheric Physics of the Chinese Academy of Sciences for his help about the use of the 325m tower data.This work was supported by the National Key Research and Development Program of China

30 (2017YFC0209605,) and the National Natural Science Foundation of China (Grant Nos. 11472272).

References

Al-Jiboori, M. H. and Fei, H.: Surface roughness around a 325-m meteorological tower and its effect on urban turbulence, Advances in Atmospheric Sciences, 22, 595–605, https://doi.org/10.1007/BF02918491, 2005.

Allwine, K. J., Shinn, J. H., Streit, G. E., Clawson, K. L., and Brown, M.: OVERVIEW OF URBAN 2000 A Multiscale Field Study of
5   Dispersion through an Urban Environment, Bulletin of the American Meteorological Society, 83, 521–536, https://doi.org/10.1175/1520-0477(2002)083<0521:OOUAMF>2.3.CO;2, 2002.

Andreas, E. L., Claffey, K. J., and Makshtas, A. P.: Low-Level Atmospheric Jets And Inversions Over The Western Weddell Sea, Boundary-Layer Meteorology, 97, 459–486, https://doi.org/10.1023/A:1002793831076, 2000.

Banta, R. M.: Stable-boundary-layer regimes from the perspective of the low-level jet, Acta Geophysica, 56, 58–87,
10   https://doi.org/10.2478/s11600-007-0049-8, 2008.

Baumbach, G. and Vogt, U.: Influence of Inversion Layers on the Distribution of Air Pollutants in Urban Areas, Water, Air, and Soil Pollution: Focus, https://doi.org/10.1023/A:1026098305581, 2003.

Boers, R. and Eloranta, E. W.: Lidar measurements of the atmospheric entrainment zone and the potential temperature jump across the top of the mixed layer, Boundary-Layer Meteorology, 34, 357–375, https://doi.org/10.1007/BF00120988, 1986.

15   Bravo-Aranda, J. A., de Arruda Moreira, G., Navas-Guzmán, F., Granados-Muñoz, M. J., Guerrero-Rascado, J. L., Pozo-Vázquez, D., Arbizu-Barrena, C., Reyes, F. J. O., Mallet, M., and Arboledas, L. A.: A new methodology for PBL height estimations based on lidar depolarization measurements: analysis and comparison against MWR and WRF model-based results, Atmospheric Chemistry and Physics, 17, 6839–6851, https://doi.org/10.5194/acp-17-6839-2017, 2017.

Brook, R. D., Franklin, B., Cascio, W., Hong, Y., Howard, G., Lipsett, M., Luepker, R., Mittleman, M., Samet, J., Smith, S. C., and Tager,
20   I.: Air pollution and cardiovascular disease: A statement for healthcare professionals from the expert panel on population and prevention science of the American Heart Association, Circulation, 109, 2655–2671, https://doi.org/10.1161/01.CIR.0000128587.30041.C8, 2004.

Brooks, I. M.: Finding Boundary Layer Top: Application of a Wavelet Covariance Transform to Lidar Backscatter Profiles, Journal of Atmospheric and Oceanic Technology, 20, 1092–1105, https://doi.org/10.1175/1520-0426(2003)020<1092:FBLTAO>2.0.CO;2, 2003.

Cao, J. J., Lee, S. C., Ho, K. F., Zou, S. C., Fung, K., Li, Y., Watson, J. G., and Chow, J. C.: Spatial and seasonal variations of
25   atmospheric organic carbon and elemental carbon in Pearl River Delta Region, China, Atmospheric Environment, 38, 4447–4456, https://doi.org/10.1016/j.atmosenv.2004.05.016, 2004.

Chan, C. K. and Yao, X.: Air pollution in mega cities in China, Atmospheric Environment, 42, 1 – 42, https://doi.org/https://doi.org/10.1016/j.atmosenv.2007.09.003, 2008.

Chen, Y., An, J., Sun, Y., Wang, X., Qu, Y., Zhang, J., Wang, Z., and Duan, J.: Nocturnal Low-levelWinds and Their Impacts on Particulate
30   Matter over the Beijing Area, Advances in Atmospheric Sciences, 35, 1455–1468, https://doi.org/10.1007/s00376-018-8022-9, 2018.

Cohn, S. A. and Angevine, W. M.: Boundary Layer Height and Entrainment Zone Thickness Measured by Lidars and Wind-Profiling Radars., Journal of Applied Meteorology, 39, 1233–1247, https://doi.org/10.1175/1520-0450(2000)039<1233:BLHAEZ>2.0.CO;2, 2000.

Davis, K. J., Gamage, N., Hagelberg, C. R., Kiemle, C., Lenschow, D. H., and Sullivan, P. P.: An Objective Method for Deriving Atmospheric Structure from Airborne Lidar Observations, Journal of Atmospheric and Oceanic Technology, 17, 1455–1468,
35   https://doi.org/10.1029/RG014i002p00215, 2000.

Devara, P. C. S., Raj, P. E., Murthy, B. S., Pandithurai, G., Sharma, S., and Vernekar, K. G.: Intercomparison of Nocturnal Lower-Atmospheric Structure Observed with Lidar and Sodar Techniques at Pune, India, Journal of Applied Meteorology, 34, 1375–1383, 1995.

Ding, A. J., Fu, C. B., Yang, X. Q., Sun, J. N., Petäjä, T., Kerminen, V. M., Wang, T., Xie, Y., Herrmann, E., Herrmann, E., Zheng, L. F., Nie, W., Liu, Q., Wei, X. L., and Kulmala, M.: Intense atmospheric pollution modifies weather: a case of mixed biomass burning with fossil fuel combustion pollution in eastern China, Atmospheric Chemistry and Physics, 13, 10 545–10 554, https://doi.org/10.5194/acpd-13-14377-2013, 2013.

5   Ding, A. J., Huang, X., Nie, W., Sun, J. N., Kerminen, V., Petäjä, T., Su, H., Cheng, Y. F., Yang, X., Wang, M. H., Chi, X. G., Wang, J. P., Virkkula, A., Guo, W. D., Yuan, J., Wang, S. Y., Zhang, R. J., Wu, Y. F., Song, Y., Zhu, T., Zilitinkevich, S., Kulmala, M., and Fu, C. B.: Enhanced haze pollution by black carbon in megacities in China, Geophysical Research Letters, 43, 2873–2879, https://doi.org/10.1002/2016GL067745, 2016.

Fisher, B., Kukkonen, J., and Schatzmann, M.: Meteorology applied to urban air pollution problems: COST 715, International Journal of
10   Environment and Pollution, 16, 560–570, https://doi.org/10.1504/IJEP.2001.000650, 2001.

Flamant, C., Pelon, J., Flamant, P. H., and Durand, P.: LIDAR DETERMINATION OF THE ENTRAINMENT ZONE THICKNESS AT THE TOP OF THE UNSTABLE MARINE ATMOSPHERIC BOUNDARY LAYER, Boundary-Layer Meteorology, 83, 247–284, https://doi.org/10.5194/acpd-13-14377-2013, 1997.

Fu, Q., Zhuang, G., Wang, J., Xu, C., Huang, K., Li, J., Hou, B., Lu, T., and Streets, D. G.: Mechanism of formation of
15   the heaviest pollution episode ever recorded in the Yangtze River Delta, China, Atmospheric Environment, 42, 2023–2036, https://doi.org/10.1016/j.atmosenv.2007.12.002, 2008.

Gao, Y., Zhang, M., Liu, Z., Wang, L., Wang, P., Xia, X., Tao, M., and Zhu, L.: Modeling the feedback between aerosol and meteorological variables in the atmospheric boundary layer during a severe fog-haze event over the North China Plain, Atmospheric Chemistry and Physics,15,8(2015-04-24), 15, 1093–1130, https://doi.org/10.5194/acp-15-4279-2015, 2015.

20   Grimsdell, A. W. and Angevine, W. M.: Convective Boundary Layer Height Measurement with Wind Profilers and Comparison to Cloud Base, Journal of Atmospheric and Oceanic Technology, 15, 1331, https://doi.org/10.1175/1520-0426(1998)015<1331:CBLHMW>2.0.CO;2, 1998.

Guo, X., Sun, Y., and Miao, S.: Characterizing Urban Turbulence Under Haze Pollution: Insights into Temperature–Humidity Dissimilarity, Boundary-Layer Meteorology, 158, 501–510, https://doi.org/10.1007/s10546-015-0104-y, 2016.

25   Han, S., Liu, J., Hao, T., Zhang, Y., Li, P., Yang, J., Wang, Q., Cai, Z., Yao, Q., Zhang, M., and Wang, X.: Boundary layer structure and scavenging effect during a typical winter haze-fog episode in a core city of BTH region, China, Atmospheric Environment, 179, 187–200, https://doi.org/10.1016/j.atmosenv.2018.02.023, 2018.

Hennemuth, B. and Lammert, A.: Determination of the Atmospheric Boundary Layer Height from Radiosonde and Lidar Backscatter, Boundary-Layer Meteorology, 120, 181–200, https://doi.org/10.1007/s10546-005-9035-3, 2006.

30   Hooper, W. P. and Eloranta, E. W.: Lidar Measurements of Wind in the Planetary Boundary Layer: The Method, Accuracy and Results from Joint Measurements with Radiosonde and Kytoon., Journal of Applied Meteorology, 25, 990–1001, https://doi.org/10.1175/1520-0450(1986)025<0990:LMOWIT>2.0.CO;2, 1986.

Huang, R.-J., Zhang, Y., Bozzetti, C., Ho, K.-F., Cao, J.-J., Han, Y., Daellenbach, K. R., Slowik, J. G., Platt, S. M., Canonaco, F., Zotter, P., Wolf, R., Pieber, S. M., Bruns, E. A., Crippa, M., Ciarelli, G., Piazzalunga, A., Schwikowski, M., ulcin Abbaszade, G., Zimmermann, R.,
35   onke Szidat, S., Baltensperger, U., Haddad, I. E., and Prevot, H.: High secondary aerosol contribution to particulate pollution during haze events in China, Nature, 514, 218–222, https://doi.org/10.1038/nature13774, 2014.

Jiannong, Quan, Yang, Qiang, Zhang, Xuexi, Junji, Suqin, Junwang, and Meng: Evolution of planetary boundary layer under different weather conditions, and its impact on aerosol concentrations, Particuology, 11, 34–40, https://doi.org/10.1016/j.partic.2012.04.005, 2013.

Kalapureddy, M. C. R., Rao, D. N., Jain, A. R., and Ohno, Y.: Wind profiler observations of a monsoon low-level jet over a tropical Indian station, Annales Geophysicae, 25, 2125–2137, https://doi.org/10.5194/angeo-25-2125-2007, 2007.

Katul, G., Goltz, S. M., Hsieh, C.-I., Cheng, Y., Mowry, F., and Sigmon, J.: Estimation of surface heat and momentum fluxes using the flux-variance method above uniform and non-uniform terrain, Boundary-Layer Meteorology, 74, 237–260, https://doi.org/10.1007/BF00712120, 1995.

Lance, S., Raatikainen, T., Onasch, T. B., Worsnop, D. R., Yu, X. Y., Alexander, M. L., Stolzenburg, M. R., McMurry, P. H., Smith, J. N., and Nenes, A.: Aerosol mixing state, hygroscopic growth and cloud activation efficiency during MIRAGE 2006, Atmospheric Chemistry and Physics, 13, 5049–5062, https://doi.org/10.5194/acp-13-5049-2013, 2012.

Li, J., Fu, Q., Huo, J., Wang, D., Yang, W., Bian, Q., Duan, Y., Zhang, Y., Pan, J., and Lin, Y.: Tethered balloon-based black carbon profiles within the lower troposphere of Shanghai in the 2013 East China smog, Atmospheric Environment, 123, 327–338, https://doi.org/10.1016/j.atmosenv.2015.08.096, 2015.

Li, J., Sun, J., Zhou, M., Cheng, Z., Li, Q., Cao, X., and Zhang, J.: Observational analyses of dramatic developments of a severe air pollution event in the Beijing area, Atmospheric Chemistry and Physics, 18, 3919–3935, https://doi.org/10.5194/acp-18-3919-2018, 2017.

Liang, X., Miao, S., Li, J., Bornstein, R., Zhang, X., Gao, Y., Cao, X., Chen, F., Cheng, Z., Clements, C., Dabberdt, W., Ding, A., Ding, D., Dou, J. J., Dou, J. X., Dou, Y., Grimmond, C. S. B., Gonzalez-Cruz, J., He, J., Huang, M., Huang, X., Ju, S., Li, Q., Niyogi, D., Quan, J., Sun, J., Sun, J. Z., Yu, M., Zhang, J., Zhang, Y., Zhao, X., Zheng, Z., and Zhou, M.: SURF: Understanding and Predicting Urban Convection and Haze, Bulletin of the American Meteorological Society, https://doi.org/10.1175/BAMS-D-16-0178.1, 2018.

Liu, X., Zhang, Y., Cheng, Y., Hu, M., and Han, T.: Aerosol hygroscopicity and its impact on atmospheric visibility and radiative forcing in Guangzhou during the 2006 PRIDE-PRD campaign, Atmospheric Environment, 60, 59–67, https://doi.org/10.1016/j.atmosenv.2012.06.016, 2012.

Miao, Y., Guo, J., Liu, S., Zhao, C., Li, X., Zhang, G., Wei, W., and Ma, Y.: Impacts of synoptic condition and planetary boundary layer structure on the trans-boundary aerosol transport from Beijing-Tianjin-Hebei region to northeast China, Atmospheric Environment, 181, 1–11, https://doi.org/10.1016/j.atmosenv.2018.03.005, 2018.

Pichugina, Y. L. and Banta, R. M.: Stable Boundary Layer Depth from High-Resolution Measurements of the Mean Wind Profile, Journal of Applied Meteorology and Climatology, 49, 20–35, https://doi.org/10.1175/2009JAMC2168.1, 2010.

Quan, L. and Hu, F.: Relationship between turbulent flux and variance in the urban canopy, Meteorology and Atmospheric Physics, 104, 29–36, https://doi.org/10.1007/s00703-008-0012-5, 2009.

Ren, Y., Zheng, S., Wei, W., Wu, B., Zhang, H., Cai, X., and Song, Y.: Characteristics of Turbulent Transfer during Episodes of Heavy Haze Pollution in Beijing in Winter 2016/17, Journal of Meteorological Research, 32, 69–80, https://doi.org/10.1007/s13351-018-7072-3, 2018.

Seibert, P., Beyrich, F., Gryning, S. E., Joffre, S., Rasmussen, A., and Tercier, P.: Review and intercomparison of operational methods for the determination of the mixing height, Atmospheric Environment, 34, 1001–1027, https://doi.org/10.1016/S1352-2310(99)00349-0, 2000.

Seinfeld, J. H. and Pandis, S. N.: Atmospheric Chemistry and Physics: From Air Pollution to Climate Change, 1997.

Sheng, J., Zhao, D., Ding, D., Li, X., Huang, M., Gao, Y., Quan, J., and Zhang, Q.: Characterizing the level, photochemical reactivity, emission, and source contribution of the volatile organic compounds based on PTR-TOF-MS during winter haze period in Beijing, China, Atmospheric Research, 212, https://doi.org/10.1016/j.atmosres.2018.05.005, 2018.

Sorbjan, Z.: Structure of the Atmospheric boundary layer, Prentice Hall,Englewood Cliffs,N.J., 1989.

Stull, R. B.: An Introduction to Boundary Layer Meteorology, Atmospheric Sciences Library, 8, 89, 1988.

Summa, D., Girolamo, P. D., Stelitano, D., and Cacciani, M.: Characterization of the planetary boundary layer height and structure by Raman lidar: comparison of different approaches, Atmospheric Measurement Techniques, 6, 3515–3525, https://doi.org/10.5194/amt-6-3515-2013, 2013.

Sun, Y., Zhuang, G., Tang, A., Wang, Y., and An, Z.: Chemical characteristics of PM2.5 and PM10 in haze-fog episodes in Beijing., Environmental Science and Technology, 40, 3148–3155, https://doi.org/10.1021/es051533g, 2006.

Sun, Y., Jiang, Q., Wang, Z., Fu, P., Li, J., Yang, T., and Yin, Y.: Investigation of the sources and evolution processes of severe haze pollution in Beijing in January 2013, Journal of Geophysical Research, 119, 4380–4398, https://doi.org/10.1002/2014JD021641, 2014.

Sun, Y., Du, W., Wang, Q., Zhang, Q., Chen, C., Chen, Y., Chen, Z., Fu, P., Wang, Z., Gao, Z., and Worsnop, D. R.: Real-Time Characterization of Aerosol Particle Composition above the Urban Canopy in Beijing: Insights into the Interactions between the Atmospheric Boundary Layer and Aerosol Chemistry., Environmental Science and Technology, 49, 11 340–11 347, https://doi.org/10.1021/acs.est.5b02373, 2015.

Sun, Y. L., Wang, Z. F., Fu, P. Q., Yang, T., Jiang, Q., Jiang, Q., Dong, H. B., Li, J., and Jia, J. J.: Aerosol composition, sources and processes during wintertime in Beijing, China, Atmospheric Chemistry and Physics, 13, 4577–4592, https://doi.org/10.5194/acp-13-4577-2013, 2013.

Wang, H., Wang, H., Xue, M., Zhang, X. Y., Liu, H. L., Zhou, C. H., Tan, S. C., Che, H. Z., Chen, B., and Li, T.: Mesoscale modeling study of the interactions between aerosols and PBL meteorology during a haze episode in Jing–Jin–Ji (China) and its nearby surrounding region – Part 1: Aerosol distributions and meteorological features, Atmospheric Chemistry and Physics, 15, 3257–3275, https://doi.org/10.5194/acp-15-3257-2015, 2014b.

Wang, Q., Sun, Y., Xu, W., Du, W., Zhou, L., Tang, G., Chen, C., Cheng, X., Zhao, X., and Ji, D.: Vertically resolved characteristics of air pollution during two severe winter haze episodes in urban Beijing, China, Atmospheric Chemistry and Physics, 18, 1–28, https://doi.org/10.5194/acp-18-2495-2018, 2018.

Wang, Y., Klipp, C. L., Garvey, D. M., Ligon, D. A., Williamson, C. C., Chang, S. S., Newsom, R. K., and Calhoun, R.: Nocturnal Low-Level-Jet-Dominated Atmospheric Boundary Layer Observed by a Doppler Lidar Over Oklahoma City during JU2003, Journal of Applied Meteorology and Climatology, 46, 2098–2109, https://doi.org/10.1175/2006JAMC1283.1, 2007.

Wang, Y. S., Li, Y., Wang, L. L., Liu, Z. R., Dongsheng, J. I., Tang, G. Q., Zhang, J. K., Yang, S., Bo, H. U., and Xin, J. Y.: Mechanism for the formation of the January 2013 heavy haze pollution episode over central and eastern China, Science China Earth Sciences, 57, 14–25, https://doi.org/10.1007/s11430-013-4773-4, 2014a.

Wang, Z., Wang, Z., Cao, X., Zhang, L., Notholt, J., Zhou, B., Liu, R., and Zhang, B.: Lidar measurement of planetary boundary layer height and comparison with microwave profiling radiometer observation, Atmospheric Measurement Techniques, 5, 1965–1972, https://doi.org/10.5194/amtd-5-1233-2012, 2012.

Wei, W., Zhang, H., Wu, B., Huang, Y., Cai, X., Song, Y., and Li, J.: Intermittent turbulence contributes to vertical diffusion of PM2.5 in the North China Plain, Atmospheric Chemistry and Physics, pp. 1–21, https://doi.org/10.5194/acp-18-12953-2018, 2018.

Zhang, Q., Quan, J., Tie, X., Li, X., Liu, Q., Gao, Y., and Zhao, D.: Effects of meteorology and secondary particle formation on visibility during heavy haze events in Beijing, China, Science of The Total Environment, 502, 578–584, https://doi.org/10.1016/j.scitotenv.2014.09.079, 2015b.

Zhang, R., Wang, G., Guo, S., Zamora, M. L., Ying, Q., Lin, Y., Wang, W., Hu, M., and Wang, Y.: Formation of Urban Fine Particulate Matter, Chemical Reviews, 115, 3803–3855, https://doi.org/10.1021/acs.chemrev.5b00067, 2015a.

Zhang, X. Y., Wang, Y. Q., Niu, T., Zhang, X. C., Gong, S. L., Zhang, Y. M., and Sun, J. Y.: Atmospheric aerosol compositions in China: spatial/temporal variability, chemical signature, regional haze distribution and comparisons with global aerosols, Atmospheric Chemistry and Physics, 12, 779–799, https://doi.org/10.5194/acp-12-779-2012, 2011.